NJC

ROYAL SOCIETY OF CHEMISTRY

PAPER

View Article Online
View Journal | View Issue

Cite this: *New J. Chem.*, 2021, **45**, 19043

Novel coumarin–pyrazoline hybrids: synthesis, cytotoxicity evaluation and molecular dynamics study

Fatma A. Ragab,[a] Amal A. M. Eissa,[a] Samar H. Fahim, *[a] Mohammad Alaraby Salem,[bc] Mona A. Gamal[a] and Yassin M. Nissan[ab]

A novel series of coumarin–pyrazoline hybrids **3a–f**, **4a–c** and **5a–c** have been synthesized and tested for their antiproliferative activity against the breast cancer cell line MCF-7. The most active compounds **3d**, **3e**, **3f**, **5a** and **5c** were also evaluated for their ability to inhibit EGFR expression with reference to erlotinib. *In silico* studies using rigid docking, flexible docking and molecular dynamics were performed to explore the possibility of direct interactions between the active molecules and the ATP-binding site of EGFR. Most compounds demonstrated a potent cytotoxic activity against the MCF-7 cell line. The most active compounds **3d**, **3e**, **3f**, **5a** and **5c** with IC_{50} values of 5, 26, 44, 20, and 50 nM, respectively, were further tested against HCT-116, HepG-2, A549 and SGC-7901 cell lines. All the tested compounds showed better activity than the reference standard drugs (doxorubicin and erlotinib) in all the tested cell lines. Compound **5a** was the most potent one against HCT-116 with an IC_{50} value of 5 nM, while compound **3d** was the most potent one against the breast cancer cell line MCF-7, liver HepG-2, lung A549 and the gastric cancer cell line SGC-7901 with IC_{50} values of 5, 77, 27 and 60 nM, respectively. Compounds **3d** and **5a** were tested for their cytotoxic effects on the normal breast cancer cell line MCF10a and their IC_{50} values were 35.78 and 22.77 μM, respectively, indicating good selectivity. The most active compounds **3d**, **3e**, **3f**, **5a** and **5c** exhibited percent reduction in EGFR level ranging from 80.9 to 88.0%. The apoptotic effect of compounds **3d** and **5a** on MCF-7 cells was investigated through cell cycle analysis. Both compounds showed increases in the number of cells in the pre-G1 phase of 14 and 22 folds, respectively, compared to the control. Both compounds exhibited total apoptosis of 28.06 and 43.88%, respectively. Docking of the new ligands revealed high scores compared to that of erlotinib. In the case of thiourea derivatives **3d** and **3e**, more stable hydrogen bonds *via* the thiourea group were demonstrated through molecular dynamics.

Received 10th June 2021,
Accepted 14th September 2021

DOI: 10.1039/d1nj02862f

rsc.li/njc

1. Introduction

Coumarins (benzopyran-2-ones) have been found to exhibit diverse biological activities, with low toxicity levels.[1] Their antitumor activity is of particular interest especially against breast cancer cells. The natural coumarin derivative neotanshinlactone **I** revealed significant antitumor activity against two ER^+ human breast cancer cell lines and was more potent and more selective than tamoxifen.[2, 3] The coumarin derivative Sp500263 **II** is a selective estrogen receptor modulator (SERM) which binds with high affinity to ERα.[4] In addition, coumarin derivatives are also able to modulate several specific enzymes involved in estrogen production.[5–7] Irosustat **III** is a tricyclic coumarin derivative which exhibits potent inhibition of the steroid sulfatase enzyme responsible for the conversion of inactive estrone and estradiol sulfate to the biologically active unconjugated estrone and estradiol, respectively.[6,8] Irosustat is under phase II clinical trials for the treatment of breast cancer in post-menopausal women.[9,10] Furthermore, a series of imidazolyl-7-substituted coumarins **IV** have been synthesized and have exhibited aromatase inhibitory activity at the nanomolar range.[11] Another series of coumarin carboxamides **V** inhibited the growth of cancer cells that have a high level of epidermal growth factor receptor (EGFR) expression (Fig. 1).[12] EGFR is a receptor tyrosine kinase found at abnormally high levels on the surface of many types of cancer cells and plays a fundamental role in signal transduction pathways.[13]

[a] *Pharmaceutical Chemistry Department, Faculty of Pharmacy, Cairo University, El-Kasr El-Eini Street, Cairo 11562, Egypt. E-mail: samarhfmy@hotmail.com*
[b] *Pharmaceutical Chemistry Department, Faculty of Pharmacy, October University for Modern Sciences and Arts (MSA), Giza, Egypt*
[c] *School of Life and Medical Sciences, University of Hertfordshire hosted by Global Academic Foundation, New Administrative Capital, Cairo, Egypt*

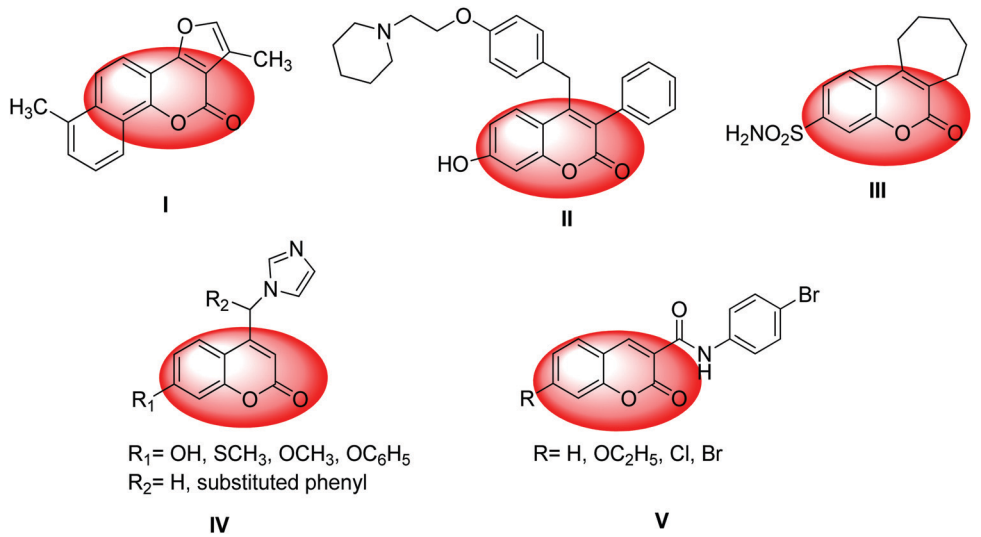

Fig. 1 Coumarin derivatives with anticancer activity.

On the other hand, the antitumor activity of pyrazoline derivatives has been widely investigated and some of these derivatives have shown potent cytotoxicity against different cancer cell lines.[14–17] In addition, 4,5-dihydropyrazoles are also considered a promising scaffold for the inhibition of EGFR.[13,18–20] Pyrazolin-1-carbothioamide **VI** and thiazolyl-pyrazoline **VII** derivatives displayed inhibitory activity against EGFR and antiproliferative activity against the MCF-7 cell line (Fig. 2).[21,22]

Moreover, thiazoline based compounds containing 2-pyrazoline framework **VIII** and coumarin-bearing 4,5-dihydropyrazoles **IX** have been recently reported to exhibit antitumor activity against the MCF-7 cell line (Fig. 2).[23,24]

Taking the biological relevance of both coumarin and pyrazoline ring systems, the present investigation deals with the synthesis of novel hybrids of coumarin and 4,5-dihydro-1*H*-pyrazoles substituted at the 1-position with thioamide, thiazole, and thiazolone skeletons aiming that these hybrids might exhibit a synergistic antitumor effect. An *in vitro* EGFR expression level assay was carried out for the most active compounds. The apoptotic effect of the most active compounds was also investigated. Furthermore, the most active derivatives were docked at the active sites of the EGFR enzyme and three representative compounds were chosen for Molecular Dynamics simulations.

2. Results and discussion

2.1. Chemistry

Precursor **1** was obtained *via* Knoevenagel condensation of salicylaldehyde and ethyl acetoacetate in the presence of piperidine.[25] The acetyl derivative **1** was converted to the corresponding chalcones **2a–f** *via* Claisen–Schmidt condensation with various aromatic aldehydes in the presence of piperidine and acetic acid[26,27] (Scheme 1). These chalcones have been utilized to synthesize different N^1-substituted pyrazolines. New coumarin–pyrazoline hybrids containing a thiourea skeleton **3a–f** have been synthesized by the reaction of **2a–f** with thiosemicarbazide under acidic conditions (Scheme 1). ^{1}H-NMR of the coumarinylpyrazolines **3a–f** showed 2 doublets of doublets at 3.23–3.47 ppm and 3.85–4.48 ppm corresponding to the two protons of the diastereotopic center C4 and a third doublet of doublets at 5.38–5.90 ppm assigned to the C5Hx. Additionally, a singlet signal appeared at 8.59–8.87 ppm assigned to the C4 proton of chromene. Protons of the phenyl substituents were observed at the expected chemical shifts and integral values. An exchangeable signal at 8.12–8.21 ppm attributed to the NH_2 protons appeared.^{13}C-NMR of **3c** exhibited signals at 44.95 and 62.95 assigned to C4 and C5 of pyrazoline, respectively, in addition to a signal at 176.64 assigned to (C═S).

Refluxing of the thioamide derivatives **3a,b,f** with monochloroacetic acid/sodium acetate in glacial acetic acid or 2-bromo-1-(4-bromophenyl)ethanone in ethanol/HCl afforded the thiazolone **4a–c** and thiazole **5a–c** derivatives, respectively. (Scheme 2). Cyclization to thiazolone was confirmed *via* ^{1}H-NMR spectra by the appearance of a singlet at 3.81–3.90 ppm attributed to the CH_2 protons of thiazolone and the disappearance of an exchangeable peak at 8.21–8.46 ppm attributed to NH_2. The formation of the thiazole derivatives **5a–c** was confirmed by ^{1}H-NMR which revealed a singlet at 6.84–6.88 ppm attributed to the CH thiazole proton and the disappearance of the exchangeable peak attributed to the NH_2 protons.

2.2. Anticancer activity

2.2.1. Antiproliferative activity. New derivatives were tested for their *in vitro* cytotoxicity against the MCF-7 breast cancer cell line. The most active derivatives were further tested against 4 different cell lines (the HCT-116 colon cancer cell line, HepG-2 hepatic cancer cell line, A549 lung cancer cell line and SGC-7901 gastric cancer cell lines) using the MTT assay.[28,29] Doxorubicin and erlotinib were used as positive controls. The activity was expressed by median growth inhibitory concentration

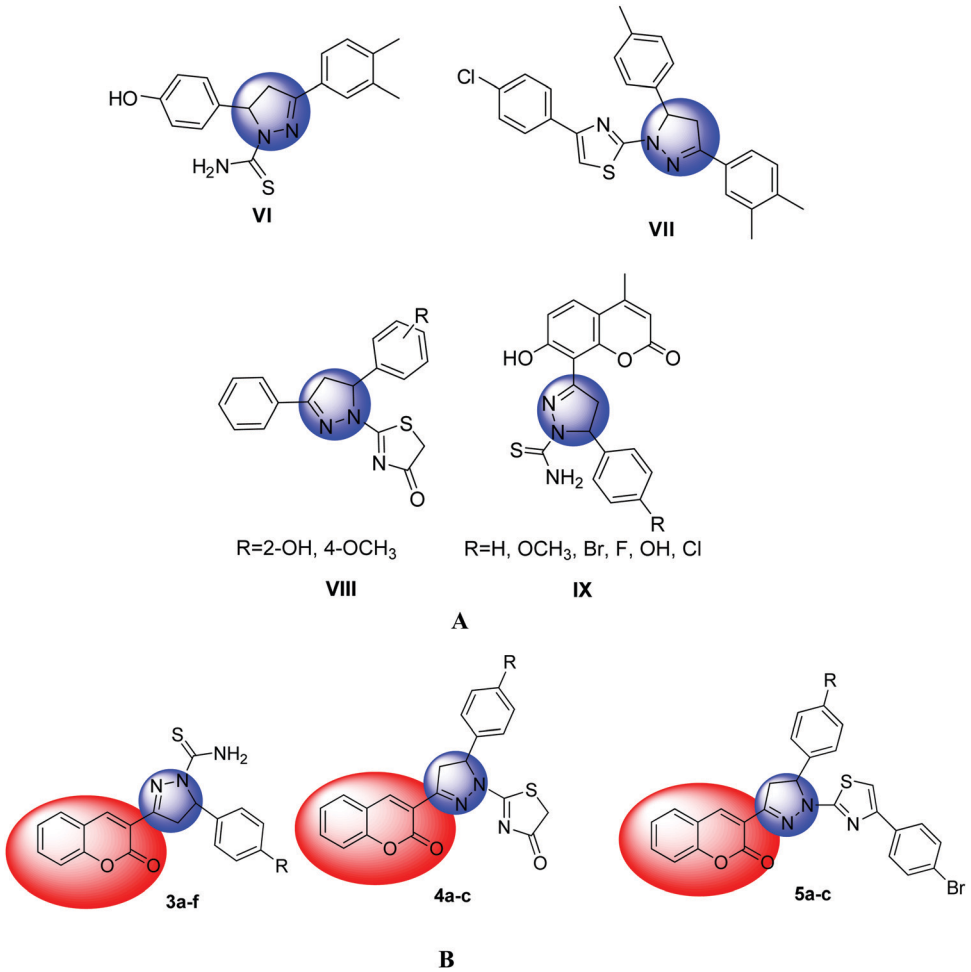

Fig. 2 (A) Pyrazoline derivatives with anticancer activity, (B) coumarin–pyrazoline hybrid strategy for final compounds **3a–f**, **4a–c** and **5a–c**.

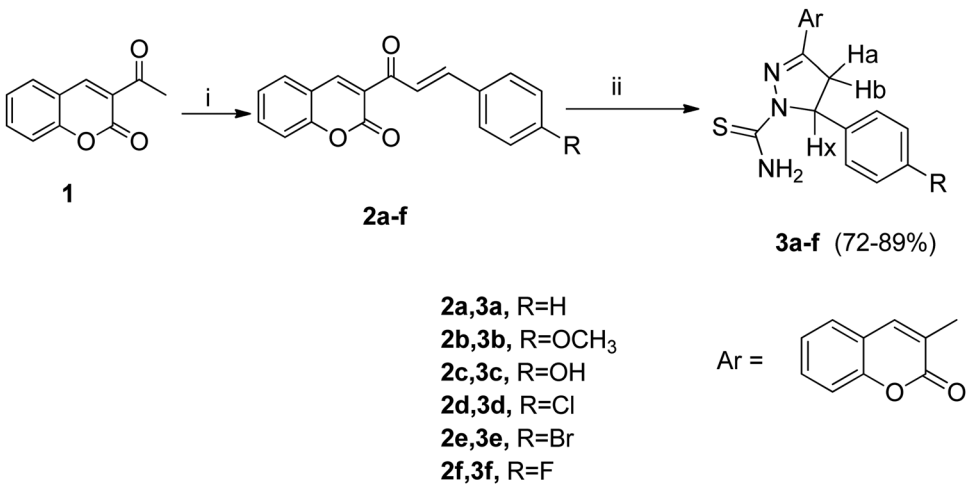

Scheme 1 Synthesis of the target compounds **2a–f–3a–f**. Reagents and conditions: (i) Ar–CHO, gl. Acetic acid–piperidine/ethanol/reflux 4 h; and (ii) thiosemicarbazide, conc. HCl/absolute ethanol/reflux 8–12 h.

(IC_{50}) and is provided in Tables 1 and 2. The results revealed that, against MCF-7, most compounds were more potent than doxorubicin with IC_{50} values ranging from 0.005–4.120 μM; the IC_{50} value of doxorubicin is 0.800 μM. All the tested compounds were more potent than erlotinib, an EGFR inhibitor (the IC_{50} value of erlotinib is 4.700 μM) (Table 1).

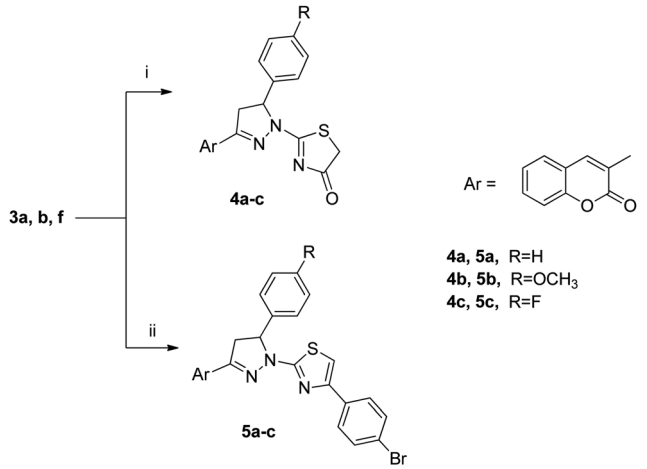

Scheme 2 Synthesis of the target compounds **4a–c–5a–c**. Reagents and conditions: (i) monochloroacetic acid, anhydrous sodium acetate, glacial acetic acid/reflux 3 h; and (ii) 2-bromo-1-(4-bromophenyl)ethanone/conc. HCl, absolute ethanol/reflux 8 h.

Table 1 The IC_{50} (μM) values of the newly synthesized coumarin derivatives against MCF-7

Compound	IC_{50} (μM)
3a	0.086
3b	0.400
3c	0.290
3d	0.005
3e	0.026
3f	0.044
4a	3.590
4b	4.120
4c	1.990
5a	0.020
5b	0.067
5c	0.050
Doxorubicin	0.800
Erlotinib	4.670

Table 2 The IC_{50} of the most active compounds against HCT-116, HepG-2, A549 and SGC-7901 cell lines

	Cell line			
	Colon HCT-116	Liver HepG-2	Lung A549	Gastric cancer cell SGC-7901
Compound	IC_{50} values (μM)			
3d	0.059	0.077	0.027	0.060
3e	0.061	0.350	0.047	0.070
3f	0.086	0.250	0.056	0.150
5a	0.005	0.690	0.049	0.061
5c	0.020	0.150	0.057	0.160
Doxorubicin	4.430	3.310	2.020	6.350
Erlotinib	2.820	3.900	3.110	20.350

All the derivatives in the **3a–f** series were more active than the standard drugs. Different substituents at the 5th position of the pyrazoline nucleus affected the activity. The *p*-chloro derivative **3d** was the most active one with an IC_{50} value of 0.005 μM while the *p*-bromo phenyl isostere **3e** showed diminished activity with an IC_{50} value of 0.026 μM. The *p*-fluoro derivative **3f** was still the least active of the three-halo derivatives with an IC_{50} of 0.044 μM. On the other hand, the *p*-methoxyphenyl **3b** and the *p*-hydroxyphenyl derivatives **3c** exhibited much more diminished activity with IC_{50} values of 0.4 μM and 0.29 μM, respectively.

The coumarin derivatives carrying 4,5-dihydro-2-(*1H*-pyrazol-1-yl)thiazol-4-one moieties **4a–c** showed good cytotoxicity but lower than the thioamide series with IC_{50} ranging from 1.99–4.12 μM. All the derivatives showed better activity than standard erlotinib but had lower cytotoxicity than doxorubicin. The most active compound was **4c** with *p*-fluorophenyl substituent in the 5th position of the pyrazoline nucleus with an IC_{50} value of 1.99 μM while its congeners with phenyl **4a** or *p*-methoxyphenyl **4b** substituent exhibited diminished activity with IC_{50} values of 3.59 μM and 4.12 μM, respectively.

The thiazole derivatives **5a–c** possessed much more increased activity than those containing a thiazolone nucleus with IC_{50} ranging from 0.02–0.06 μM and were found to be more potent than the two standard drugs. The most active derivative was the one carrying the unsubstituted phenyl **5a** with an IC_{50} value of 0.02 μM, about 3 times more active than the other two congeners the *p*-methoxyphenyl derivative **5b** and the *p*-fluorophenyl derivative **5c** with IC_{50} values of 00.067 μM and 0.05 μM, respectively.

The most active compounds, **3d**, **3e**, **3f**, **5a** and **5c**, were further tested against HCT-116, HepG-2, A549 and SGC-7901 cell lines by MTT assay. All the tested compounds showed very potent activity against the 4 tested cell lines. They were more potent than the reference drugs. Compound **5a** (IC_{50}: 5 nM) was the most potent one against colon cancer cell line HCT-116, while compound **3d** exhibited the highest cytotoxicity against HepG-2, Lung A549 and gastric SGC-7901 cell lines with IC_{50} values of 77, 27 and 60 nM, respectively.

The most active compounds **3d** and **5a** were tested for their cytotoxicity on normal breast cell line MCF10a. The IC_{50} values for both compounds were 35.78 ± 1.93 and 22.7 ± 1.23 μM, respectively, indicating good selectivity index for both compounds.

2.2.2. *In vitro* inhibition of EGFR expression. The most active derivatives **3d**, **3e**, **3f**, **5a** and **5c**, were tested for their ability to inhibit EGFR expression utilizing breast cancer cell line MCF-7 obtained from American Type Culture Collection using erlotinib as the reference drug.[30]

All the tested compounds showed excellent inhibition% of EGFR expression ranging from 80.9–88.0, but lower than erlotinib (95.68% inhibition). Compound **3d** with its *p*-chloro phenyl substituent showed the greatest activity with an inhibition% of 88.0, higher than its bromo and fluoro analogues **3e** and **3f** (inhibition% 84.6 and 84.3, respectively). Cyclization of the thioamide skeleton to a thiazole ring slightly decreased the effect as in compounds **3f** and **5c** (inhibition% 84.3 and 80.9 respectively). Interestingly, the results of the inhibition of EGFR expression level assay were almost parallel to the results of the *in vitro* cytotoxicity (Table 3).

2.2.3. Cell cycle analysis. The most active compounds **3d** and **5a** were subjected to cell cycle analysis using MCF-7 cells

Table 3 EGFR inhibitory activity of the five most active synthesized compounds

Compound no.	% Inhibition of EGFR
3d	88.00
3e	84.60
3f	84.30
5a	82.30
5c	80.90
Erlotinib	95.68

Table 4 DNA content of MCF-7 cells (treated with **3d**, **5a** and control) at 0.005 and 0.020 μM, respectively

	DNA content				
Compound no.	IC_{50}	% G0–G1	% S	% G2/M	% Pre-G1
3d/MCF7	0.005	58.19	37.22	4.59	28.06
5a/MCF7	0.02	49.93	42.19	7.88	43.88
cont. MCF7	—	55.81	34.59	9.6	2.08

using DNA content. The used concentrations in this analysis were IC_{50} values of both compounds (0.005 and 0.020 μM, respectively). The results are summarized in Table 4.

By observing the values in Table 4, we can conclude that the cell cycle arrest exerted by compound **3d** compared to control cells, with more than 28% of cells at the pre-G1 phase, had almost a 14 fold increase. A higher percentage of cells also was observed for compound **5a** at the pre-G1 phase with almost 44% of cells, having almost a 22 fold increase compared to the control.

2.2.4. Annexin V-FITC apoptosis assay. In order to investigate the apoptotic effect of the most active compounds **3d** and **5a** Annexin V-FITC/propidium iodide dual staining assay (AV/PI) was carried out by flow cytometry and the results are displayed in Fig. 3.

These results indicate that both compounds **3d** and **5a** have apoptotic potential on MCF-7 cells. In the case of compound **3d** total apoptosis was 28.06% with an early apoptosis of 3.18% and 15.22% of late apoptosis. Compound **5a** showed a more potent apoptotic behavior with total apoptosis of 43.88% with an early apoptosis of 2.59% and 26.02% of late apoptosis.

2.3. Molecular docking

Docking was performed to investigate the possibility of direct interactions between the most active compounds **3d**, **3e**, **3f**, **5a** and **5c** and the ATP-binding pocket of EGFR tyrosine kinase. The scoring results from rigid and flexible docking experiments are shown in Table 5. All the predicted scores are considerably better than that of the self-docked erlotinib, due to the limitation of docking in a dry environment, *vide infra*.

The highest score pose for ligand **3e** is depicted in Fig. 4. Ligands **3d** and **3f** show similar binding poses. Two main interactions can be recognized: a hydrogen bond between the ligand and the side chains of Asp831 and Asn818, and an aromatic–aromatic interaction with a neighboring Phe989.

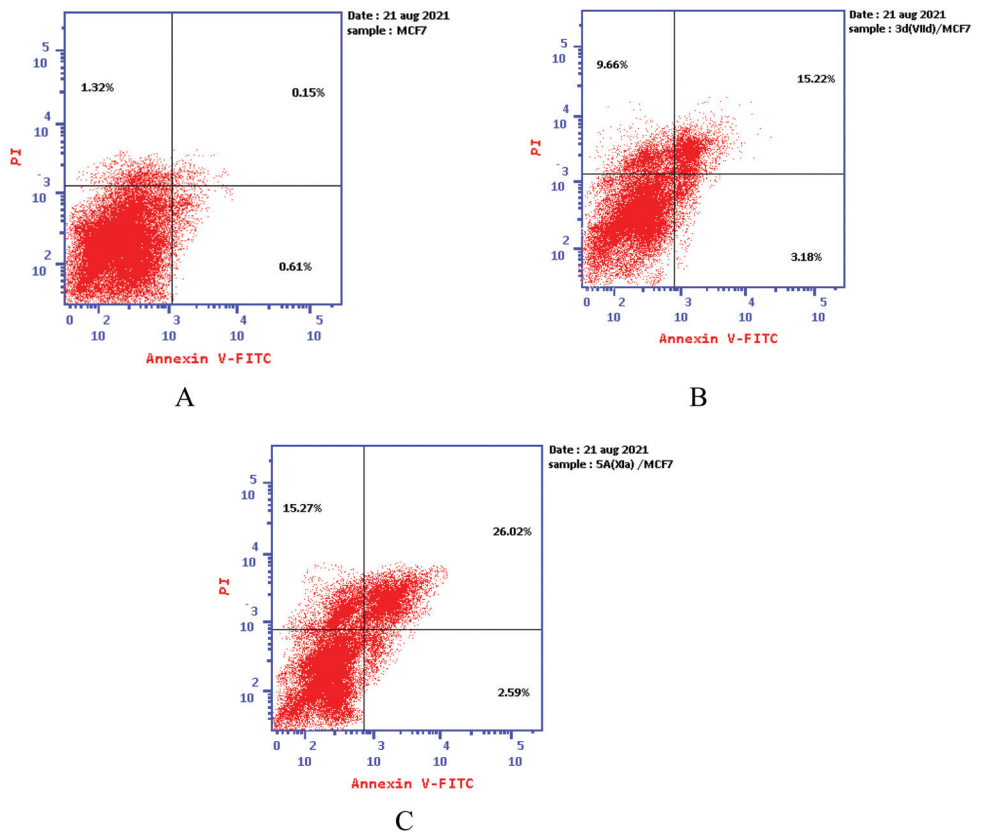

Fig. 3 Apoptotic sub-population of MCF-7 cells; untreated (A), treated with **3d** (B) and treated with **5a** (C).

Table 5 Scoring results of the five most active synthesized compounds from the rigid and flexible docking experiments

Ligand	Rigid-docking score (kcal mol^{-1})	Flexible-docking score (kcal mol^{-1})
3d	−8.6	−9.2
3e	−8.6	−10.3
3f	−8.6	−9.0
5a	−9.9	−10.8
5c	−10.2	−11.2
Erlotinib	−7.7	−7.9

Water-bridged hydrogen bonds are not considered in the current docking experiment which can result in underestimating the binding affinity. This argument is similar to the one made by Wissner *et. al.*[31] for the binding mode of erlotinib which was later validated *via* the crystal structure.[32] Interestingly, the halo-phenyl ring is the most exposed part of the **3d**, **3f** and **3e** ligands. Being exposed to solution, there is an associated solvation penalty. This penalty decreases if the exposed part of the ligand is capable of forming favorable interactions with water; *i.e.*, favorable enthalpic contribution. As the size of the halogen increases (from F to Br), its polarizability increases and thus forms stronger London Dispersion Forces with water. This trend is reflected in the scores from flexible docking.

There are many suggested poses for ligands **5a** and **5c**. The pose with the highest score for ligand **5a** is depicted in Fig. 5. Two main interactions can be observed: a hydrogen bond with the backbone nitrogen of Met769 and a H-aromatic interaction with Leu694. Ligand **5c** shows a similar binding pose. This rationalizes the high score associated with ligands **5a** and **5c** in the docking experiment. It seems that the additional aryl moiety in these two derivatives does not contribute to any major interactions.

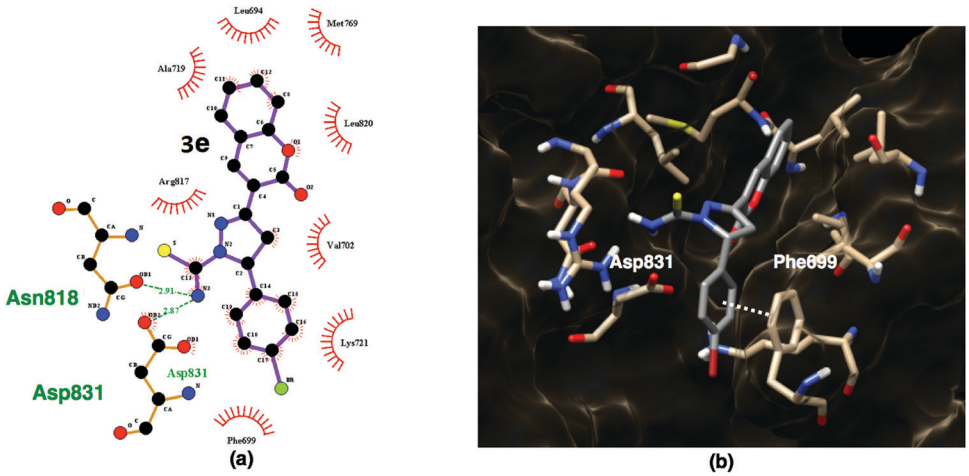

Fig. 4 Depiction of the highest-energy binding pose of **3e** in 2D and 3D according to the flexible-docking experiment.

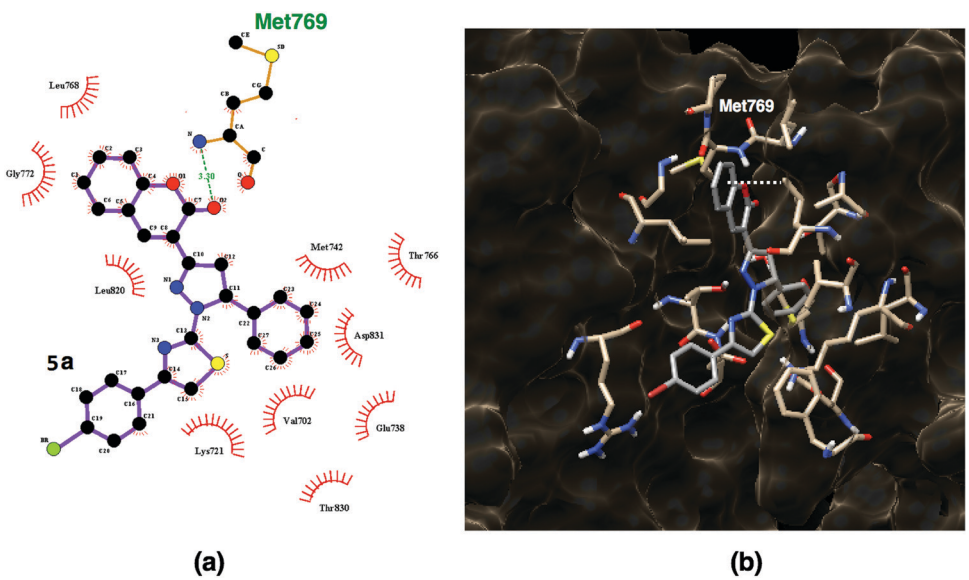

Fig. 5 Depiction of the highest-score binding pose of **5a** in 2D and 3D according to the flexible-docking experiment.

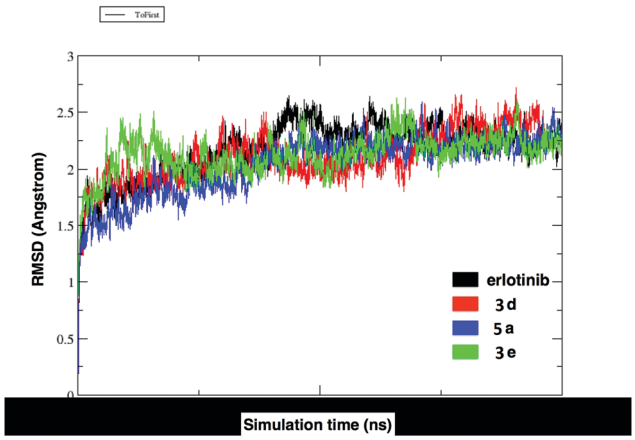

Fig. 6 RMSD of the 20 ns trajectory for the tyrosine kinase in complex with erlotinib, **3d**, **3e** and **5a**. The resolution of the crystal structure used is 2.6 Å.

Table 6 Hydrogen-bond analysis for the 14 ns of the respective MD trajectories, see Fig. 8. Lifetime refers to the percentage of snapshots in which the relevant hydrogen bond is formed. The dash designates little incidence of hydrogen bonds; lifetime less than 10%

	Life time of H-bond			
Contributing amino acid	Erlotinib	3d	3e	5a
Met769	23%		—	—
ASP831	—	37%	59%	—
CYS773	15%	—	—	—
Water bridge to THR830	24%	—	—	—
Water bridge to THR766	18%	—	—	—
Water bridge to GLU738	—	14%	40%	—

The docking poses and the possibility of forming water-bridged hydrogen bonds are further investigated *via* molecular dynamics.

2.4. Molecular dynamics (MD)

The following ligands were considered in the MD simulations in complex with the protein: **3d**, **3e**, **5a** and erlotinib. The root-mean-square-deviation (RMSD) plots for the four trajectories are illustrated in Fig. 6. The details of major H-bond contributions are given in Table 6 and Fig. 7 and 8.

2.4.1. RMSD analysis. The overall RMSD fluctuation for the protein in complex with **3d**, **3e** and **5a** is similar to that of the complex with erlotinib. The fluctuation is within the range of the crystal structure resolution, 2.6 Å, which shows the adequate stability of the dynamics simulation and that the conformations assumed by the flexible side chains are properly tolerated within the conformational space of the protein. The RMSD equilibrates early in the simulation at around 6 ns, so the trajectory between 6 and 20 ns can be used to study the protein–ligand interactions.

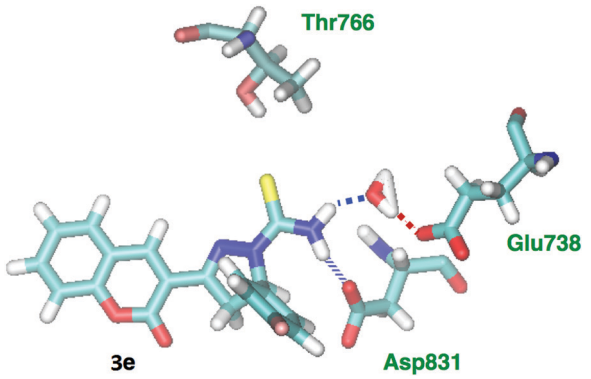

Fig. 8 Depiction of the interactions between **3e** and the active sites of the tyrosine kinase as per one snapshot in the production phase. The snapshot was chosen to demonstrate the H-bonds.

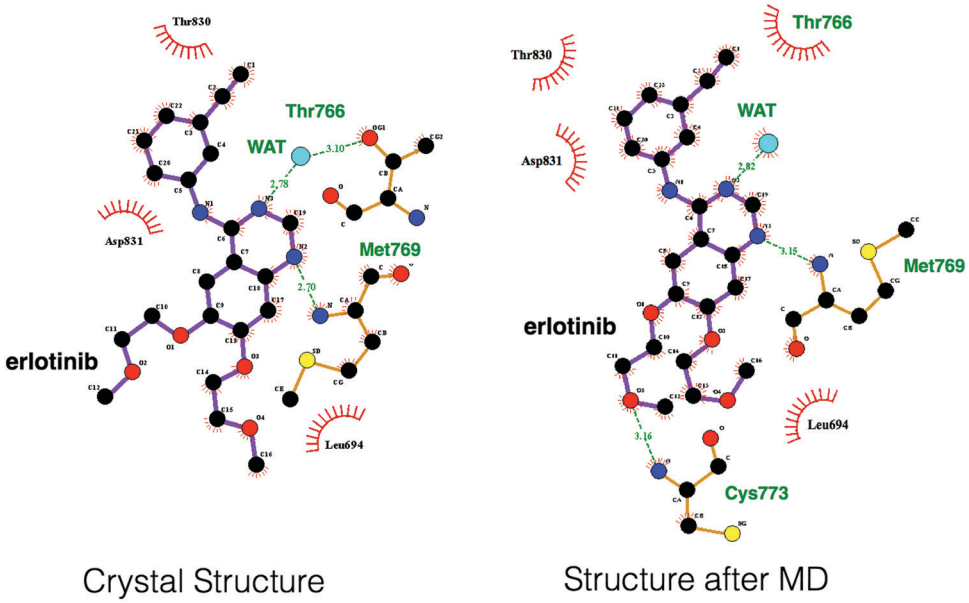

Fig. 7 Depiction of the interactions between erlotinib and the active sites of the tyrosine kinase in the native crystal structure, left, and close to the end of the molecular dynamics simulation, right.

2.4.2. H-bond analysis. The H-bonds that are formed in more than 10% of the 14 ns trajectory are given along with their lifetimes in Table 6. The average lengths and angles of the hydrogen bonds between each ligand and the surrounding amino acids are comparable and thus the argument can be focused on the number and lifetime of interactions.

The trajectory for the erlotinib–kinase complex serves as the control for our dynamics studies. As illustrated in Fig. 7 and Table 6, there are some variations between the interaction map before and after dynamics simulation. This is not unexpected, since erlotinib was not actually co-crystallized with the protein. Rather, after crystal formation, erlotinib was allowed to bind the ATP binding-site in the crystal, as reported by Stamos *et al.*[32]

For **3e**, the interaction with Asp, as depicted in Fig. 4, is further confirmed through molecular dynamics. The lifetime of the H-bond is greater than that of erlotinib with Met769 or Cys773. Another hydrogen bond that shows up in 40% of the frames is formed *via* bridging water molecules. This is equivalent to the sum of lifetimes of similar H-bonds in the case of erlotinib. The hydrogen bond network of **3d** follows the same pattern as that of **3e**, albeit with a slightly shorter lifetime. Similar to the docking results, the H-bond analysis from MD suggests that **3e** should have better binding affinity to the target than **3d**. For **5a**, no significant H-bonds are formed and thus it interacts only through other types of interactions including hydrophobic and H-aromatic interactions.

In summary, together the docking and MD studies provide a model that predicts the possibility of direct interaction between the newly synthesized ligands and the ATP-binding site of the EGFR tyrosine kinase. The docking study showed high scoring values for the new ligands with the thiourea-containing ligands (**3d**, **3e**, **3f**) having lower docking scores than the **5** series compounds. The MD study reveals an extra significant H-bond interaction for the thiourea-containing compounds which was missed in the docking experiment. Therefore, the docking score for the thiourea-containing compounds was underestimated. The cyclization of the thiourea derivative into thiazole analogues disfavors the proper orientation to make H-bonds with the amino acids in the active sites. The underestimated self-docking score of erlotinib is due to the overlooked H-bonds that were demonstrated in the molecular dynamics simulation.

3. Conclusion

A novel series of coumarin–pyrazoline hybrids **3a–f**, **4a–c** and **5a–c** were synthesized and evaluated for their anticancer activity. All the synthesized compounds demonstrated potent activity against the MCF-7 cell line. Compounds **3d** and **5a** showed good selectivity when tested on the normal cell line MCF10a. The most active compounds **3d**, **3e**, **3f**, **5a** and **5c** were further tested against HCT-116, HepG-2, A549 and SGC-7901 cell lines and showed very potent activity against the 4 tested cell lines which is even higher than those of the reference standards, doxorubicin and erlotinib. Compounds **5a** and **5c** possessed superior activity at low nanomolar levels with IC_{50} values of 20 and 21 nM, respectively, against HCT-116. The most active compounds **3d**, **3e**, **3f**, **5a** and **5c** were studied for their ability to inhibit EGFR expression where the percent reduction in EGFR ranged from 80.9 to 88.0%. Compounds **3d** and **5a** showed a potent apoptotic effect on MCF-7 cells with 28.06 and 43.88%, respectively. In addition, docking and MD studies demonstrate that, at least for the thiourea-containing derivatives, there is a possibility of having a direct interaction with the active sites of the EGFR tyrosine kinase.

4. Experimental

4.1. Chemistry

Unless otherwise noted, all materials were obtained from commercial suppliers and used without further purification. TLC was monitored on FLUKA silica gel TLC aluminium cards (0.2 mm thickness) using a fluorescence indicator at 254 nm using chloroform : methanol (9 : 1) as the eluent. Melting points were obtained using an Electrothermal 9100 melting point apparatus and were uncorrected. Elemental microanalyses were performed at the Regional Center for Microbiology and Biotechnology, Al-Azhar University. NMR spectra were recorded using a Bruker spectrophotometer at 400 MHz for ^{1}H NMR, and at 100 MHz for ^{13}C NMR and a Varian mercury 300BB at 300 MHz for ^{1}H NMR, and at 75.45 MHz for ^{13}C NMR; tetramethylsilane (TMS) was used as the internal reference. Chemical shift values were given in ppm. Mass spectra were obtained using a Fennigan MAT, SSQ 7000 mass spectrophotometer at 70eV. Infrared spectra were recorded using a Shimadzu FT-IR 8400S spectrophotometer (Shimadzu, Kyoto, Japan), and expressed in wave number (cm^{-1}), using potassium bromide discs.

4.1.1. 3-Acetyl-2*H*-chromene-2-one (1). Compound **1** was prepared according to the literature procedure (m.p. 120 °C, as reported).[25]

4.1.2. General procedure for the synthesis of 3-(arylacryloyl)-2*H*-chromene-2-one (2a–f). Compounds of this series (**2a–f**) were prepared according to the literature procedure.[27]

4.1.3. General procedure for the synthesis of 3-(2-oxo-2*H*-chromene-3-yl)-5-(4-(un)substituted phenyl)-4,5-dihydro-1*H*-pyrazole-1-carbothioamide (3a–f). A mixture of the corresponding chalcone **2a–f** (2.76 g, 10 mmol), thiosemicarbazide (0.91 g, 10 mmol) and concentrated hydrochloric acid (1 mL) was refluxed in ethanol for 12 hours (TLC). The precipitate was collected, left to dry and crystallized from DMF/ethanol.

*4.1.3.1 3-(2-Oxo-2H-chromene-3-yl)-5-phenyl-4,5-dihydro-1H-pyrazole-1-carbothioamide (**3a**):.* Yield %: 74, m.p 168–170 °C. IR ν_{max} cm^{-1}: 3350, 3170 (NH_2), 2920 (CH aliphatic), 1730 (C═O), 1602, 1510 (C═C, C═N), 1210 (C═S). ^{1}H-NMR (DMSO-d_6 400 MHz) δ ppm: 3.40 (dd, 1H, C4–H_B pyrazoline, J_{BX} = 6.7 Hz, J_{BA} = 11.5 Hz), 4.48 (dd, 1H, C4–H_A pyrazoline, J_{AX} = 4.44 Hz, J_{AB} = 11.5 Hz), 5.38 (dd, 1H, C5–H_X pyrazoline, J_{XA} = 4.4 Hz, J_{XB} = 6.7 Hz), 7.23 (t, 1H, Ar–H), 7.30 (t, 2H, Ar–H, J = 7.5), 7.38–7.42 (m, 2H, C5–H chromene and C6–H

chromene), 7.52 (d, 2H, Ar–H, J = 7.6 Hz), 7.73 (t, 1H, C7–H chromene, J = 7.12 Hz), 7.82 (d, 1H, C8–H chromene, J = 8.4 Hz), 8.59 (s, 1H, C4–H chromene), 8.64 (s, 2H, NH_2, D_2O exch.). Anal. Calculated for $C_{19}H_{15}N_3O_2S$ (349.41): C, 65.31; H, 4.33; N, 12.03. Found: C, 65.49; H, 4.41; N, 12.21.

*4.1.3.2 5-(4-Methoxyphenyl)-3-(2-oxo-2H-chromene-3-yl)-4,5-dihydro-1H-pyrazole-1-carbothio-amide (**3b**):.* Yield %: 89, m.p 180–183 °C. IR ν_{max} cm^{-1}: 3260, 3171 (NH_2), 2932 (CH aliphatic), 1727(C═O), 1602, 1587 (C═C, C═N), 1200 (C═S). ^{1}H-NMR (DMSO-d_6 400 MHz), δ ppm: 3.23 (dd, 1H, C4–H_A pyrazoline, J_{AX} = 2.2 Hz, J_{AB} = 18.6 Hz), 3.72 (S, 3H, OCH_3), 3.91 (dd, 1H, C4–H_B pyrazoline, J_{BX} = 11.4 Hz, J_{BA} = 18.6 Hz), 5.86 (dd, 1H, C5–H_X pyrazoline, J_{XA} = 2.1 Hz, J_{XB} = 11.4 Hz), 6.87 (d, 2H, Ar–H, J = 8.16 Hz), 7.08 (d, 2H, Ar–H, J = 8.16 Hz), 7.39–7.45 (m, 2H, C5–H chromene and C6–H chromene), 7.69 (t, 1H, C7–H chromene, J = 7.6 Hz), 7.81 (d, 1H, C8–H chromene, J = 7.6 Hz), 7.86 (s, 1H, SH, D_2O exch.), 8.17 (s, 1H, NH, D_2O exch.), 8.78(s, 1H, C4–H chromene). Anal. Calculated for $C_{20}H_{17}N_3O_3S$ (379.43): C, 63.31; H, 4.52; N, 11.07. Found: C, 63.47; H, 4.60; N, 11.34. MS: m/z 379.14, M^+, 44.08 (100%).

*4.1.3.3 5-(4-Hydroxyphenyl)-3-(2-oxo-2H-chromene-3-yl)-4,5-dihydro-1H-pyrazole-1-carbothio-amide (**3c**):.* Yield %: 72, m.p 182–184 °C. IR ν_{max} cm^{-1}: 3260, 3171(NH_2), 3340 (OH), 2927 (CH aliphatic), 1718 (C═O), 1600, 1590 (C═C, C═N), 1200 (C═S). ^{1}H-NMR (DMSO-d_6 400 MHz) δ ppm: 3.32 (dd, 1H, C4–H_A pyrazoline, J_{AX} = 3.3 Hz, J_{AB} = 18.6 Hz), 3.89 (dd, 1H, C4–H_B pyrazoline, J_{BX} = 11.4 Hz, J_{BA} = 18.6 Hz), 5.80 (dd, 1H, C5–H_X pyrazoline, J_{XA} = 3.3 Hz, J_{XB} = 11.4 Hz), 6.69 (d, 2H, Ar–H, J = 8.5 Hz), 6.95 (d, 2H, Ar–H, J = 8.6 Hz), 7.40–7.49 (m, 2H, C5–H chromene and C6–H chromene), 7.75 (t, 1H, C7–H chromene, J = 7.2 Hz), 7.78 (d, 1H, C8–H chromene, J = 7.2 Hz), 7.82 (s, 1H, SH, D_2O exch.), 8.12 (s, 1H, NH, D_2O exch.), 8.84 (s, 1H, C4–H chromene), 9.34 (s, 1H, OH, D_2O exch.), ^{13}C-NMR (DMSO 100.63 MHz): 44.95 (C-4 pyrazoline), 62.95 (C-5 pyrazoline), 115.57, 116.62, 119.23, 119.32, 125.54, 127.09, 129.65, 133.59, 133.60, 142.64, 151.87, 154.82, 156.80 (aromatic C), 158.23 (carbonyl), 176.64 (C═S). Calculated for $C_{19}H_{15}N_3O_3S$ (365.41): C, 62.45; H, 4.14; N, 11.50. Found: C, 62.50; H, 4.23; N, 11.61.

*4.1.3.4 5-(4-Chlorophenyl)-3-(2-oxo-2H-chromene-3-yl)-4,5-dihydro-1H-pyrazole-1-carbothio-amide (**3d**):.* Yield %: 75, m.p 165–167 °C. IR ν_{max} cm^{-1}: 3290, 3180 (NH_2), 2931 (CH aliphatic), 1731(C═O), 1602, 1587 (C═C, C═N), 1200 (C═S). ^{1}H NMR (DMSO-d_6 400 MHZ), δ ppm: 3.43 (dd, 1H, C4–H_A pyrazoline, J_{AX} = 3.7 Hz, J_{AB} = 16.9 Hz), 4.35 (dd, 1H, C4–H_B pyrazoline, J_{BX} = 11.2 Hz, J_{BA} = 16.9 Hz), 5.42 (dd, 1H, C5–H_X pyrazoline, J_{XA} = 3.7 Hz, J_{XB} = 11.2 Hz), 6.78 (d, 2H, Ar–H, J = 8.3 Hz), 6.92 (d, 2H, Ar–H, J = 8.3 Hz), 7.31 (m, 2H, C5–H chromene and C6–H chromene), 7.65 (t, 1H, C7–H chromene, J = 7.4 Hz), 7.82 (d, 1H, C8–H chromene, J = 7.4 Hz), 8.31 (s, 2H, NH_2, D_2O exch.), 8.85 (s, 1H, C4–H chromene), Anal. Calculated for $C_{19}H_{14}ClN_3O_2S$ (383.85): C, 59.45; H, 3.68;N, 10.95. Found: C, 59.63; H, 3.74; N, 11.12.

*4.1.3.5 5-(4-Bromophenyl)-3-(2-oxo-2H-chromene-3-yl)-4,5-dihydro-1H-pyrazole-1-carbothio-amide (**3e**):.* Yield: 75%, m.p 170–172 °C. IR ν_{max} cm^{-1}: 3260, 3171(NH_2), 2932 (CH aliphatic), 1720 (C═O of coumarin), 1602, 1587 (C═C, C═N), 1207 (C═S). ^{1}H-NMR (DMSO-d_6 400 MHz), δ ppm: 3.47 (dd, 1H, C4–H_A pyrazoline, J_{AX} = 4.4 Hz, J_{AB} = 18.2 Hz), 3.85 (dd, 1H, C4–H_B pyrazoline, J_{BX} = 12.1 Hz, J_{BA} = 18.2 Hz), 5.81 (dd, 1H, C5–H_X pyrazoline, J_{XA} = 4.4 Hz, J_{XB} = 12.2 Hz), 6.68 (d, 2H, Ar–H, J = 8.1 Hz), 6.83 (d, 2H, Ar–H, J = 8.1 Hz), 7.41 (m, 2H, C5–H chromene and C6–H chromene), 7.71 (t, 1H, C7–H chromene, J = 7.6 Hz), 7.82 (d, 1H, C8–H chromene, J = 7.26 Hz), 8.11 (s, 2H, NH_2, D_2O exch.), 8.7 (s, 1H, C4–H chromene), Anal. Calculated for $C_{19}H_{14}BrN_3O_2S$ (428.30): C, 53.28; H, 3.29; N, 9.8. Found: C, 53.41; H, 3.37; N, 9.97.

*4.1.3.6 5-(4-Fluorophenyl)-3-(2-oxo-2H-chromene-3-yl)-4,5-dihydro-1H-pyrazole-1-carbothio-amide (**3f**):.* Yield: 75%, m.p. 169–171 °C. IR ν_{max} cm^{-1}: 3244, 3172 (NH_2), 2930 (CH aliphatic), 1722 (C═O), 1602, 1580 (C═C, C═N), 1200 (C═S). ^{1}H-NMR (DMSO-d_6 400 MHz), δ ppm: 3.23 (dd, 1H, C4–H_A pyrazoline, J_{AX} = 3.6 Hz, J_{AB} = 18.8 Hz), 3.95 (dd, 1H, C4–H_B pyrazoline, J_{BX} = 11.6Hz, J_{BA} = 18.8 Hz), 5.90 (dd, 1H, C5–H_X pyrazoline, J_{XA} = 3.6 Hz, J_{XB} = 11.6 Hz), 7.15 (d, 2H, Ar–H, J = 8.8 Hz), 7.18 (d, 2H, Ar–H, J = 8.8 Hz), 7.41–7.46 (m, 2H, C5–H chromene and C6–H chromene), 7.68 (t, 1H, C7–H chromene, J = 7.7 Hz), 7.76 (d, 1H, C8–H chromene, J = 7.7 Hz), 8.21 (s, 2H, NH_2, D_2O exch.), 8.87 (s, 1H, C4–H chromene). Anal. Calculated for $C_{19}H_{14}FN_3O_2S$ (367.40): C, 62.11; H, 3.84; N, 11.44. Found: C, 62.37; H, 3.88; N, 11.61.

4.1.4. General procedure for the synthesis of 2-[3-(2-oxo-2*H*-chromene-3-yl)-5-(4-(Un)substituted phenyl)-4,5-dihydro-1*H*-pyrazol-1-yl]thiazol-4(5*H*)-one (4a–c):. A mixture of the appropriate thiocarbomoyl-pyrazoline derivative **3a,b,f** (10 mmol), chloroacetic acid (0.94 g, 10 mmol) and anhydrous sodium acetate (0.3 g, 10 mmol) was heated under reflux conditions in glacial acetic acid (15 mL) for 3 h. It was allowed to cool, and the reaction mixture was poured on ice water. The precipitate formed was filtered, dried and crystallized from ethanol.

*4.1.4.1 2-[3-(2-oxo-2H-chromene-3-yl)-5-phenyl-4,5-dihydro-1H-pyrazol-1-yl]thiazol-4(5H)-one (**4a**):.* Yield %: 83, m.p. 231–233 °C. IR ν_{max} cm^{-1}: 2933 (CH aliphatic), 1726 (C═O), 1710 (C═O thiazolone), 1602, 1510 (C═C, C═N). ^{1}H-NMR ($CDCl_3$ 400 MHz), δ ppm: 3.67 (dd, 1H, C4–H_A pyrazoline, J_{AX} = 3.8 Hz, J_{AB} = 19.3 Hz), 3.90 (s, 2H, H of CH_2 thiazolone), 4.14 (dd, 1H, C4–H_B pyrazoline, J_{BX} = 11.4 Hz, J_{BA} = 19.3 Hz), 5.82 (dd, 1H, C5–H_X pyrazoline, J_{XA} = 3.7 Hz, J_{XB} = 11.4 Hz), 7.23 (d, 2H, Ar–H, J = 7.2 Hz), 7.31–7.40 (m, 5H, 3Ar–H, C5–H chromene and C6–H chromene), 7.65 (d, 1H, C8–H chromene, J = 7.5 Hz), 7.67 (dd, 1H, C7–H chromene, J = 18.1 Hz, J = 7.7 Hz), 8.60 (s, 1H, C4–H chromene). Anal. Calculated for $C_{21}H_{15}N_3O_3S$ (389.43): C, 64.77; H, 3.88; N, 10.79. Found: C, 64.56; H, 3.81; N, 10.82.

*4.1.4.2 2-[5-(4-Methoxyphenyl)-3-(2-oxo-2H-chromene-3-yl)-4,5-dihydro-1H-pyrazol-1-yl] thiazol-4(5H)-one (**4b**):.* Yield %: 83,

m.p. 240–242 °C. IR ν_{max} cm^{-1}: 2933 (CH aliphatic), 1726 (C═O), 1719 (C═O thiazolone), 1602, 1495 (C═C, C═N). ^{1}H-NMR ($CDCl_3$ 300 MHZ), δ ppm: 3.66 (dd, 1H, C4–H_A pyrazoline, J_{AX} = 3.6 Hz, J_{AB} = 19.2 Hz), 3.78 (s, 3H, OCH_3), 3.86 (s, 2H, CH_2 thiazolone), 4.12 (dd, 1H, C4–H_B pyrazoline, J_{BX} = 11.1 Hz, J_{BA} = 19.2 Hz), 5.73 (dd, 1H, C5–H_X pyrazoline, J_{XA} = 3.6 Hz, J_{XB} = 11.1 Hz), 6.85 (d, 2H, Ar–H, J = 8.7 Hz), 7.22 (d, 2H, Ar–H, J = 8.4 Hz), 7.37–7.40 (m, 2H, C5–H chromene and C6–H chromene), 7.63 (t, 1H, C7–H chromene, J = 7.8 Hz), 7.68 (d, 1H, C8–H chromene, J = 8.1 Hz), 8.57 (s, 1H, C4–H chromene). ^{13}C-NMR (DMSO 100 MHz): 38.70 (CH_2 thiazolone), 45.53 (C-4 pyrazoline), 55.59 (OCH_3), 63.54 (C-5 pyrazoline), 114.63, 116.60, 118.58, 118.98, 125.44, 127.68, 130.26, 132.74, 134.11, 144.11, 154.22, 157.62, 157.98, (aromatic C), 159.35 (C═N), 178.25, 187.42 (carbonyl). Anal. calculated for $C_{22}H_{17}N_3O_4S$ (419.45): C, 63.00; H, 4.09; N, 10.02. Found: C, 63.12; H, 4.1; N, 10.09. MS: m/z 419.1, M^+, 248 (100%).

*4.1.4.3 2-[5-(4-Fluorophenyl)-3-(2-oxo-2H-chromene-3-yl)-4,5-dihydro-1H-pyrazol-1-yl]thiazol-4(5H)-one (**4c**):.* Yield %: 90, m.p. 230–232 °C. IR ν_{max} cm^{-1}: 2933 (CH aliphatic), 1726 (C═O), 1719 (C═O thiazolone), 1602, 1495 (C═C, C═N).^{1}H-NMR ($CDCl_3$ 400 MHz), δ ppm: 3.31 (dd, 1H, C4–H_A pyrazoline, J_{AX} = 5.8 Hz, J_{AB} = 18.2 Hz), 3.81(S, 2H, CH_2 thiazolone), 3.92 (dd, 1H, C4–H_B pyrazoline, J_{BX} = 12.3 Hz, J_{BA} = 18.2 Hz), 5.81 (dd, 1H, C5–H_X pyrazoline, J_{XA} = 5.8 Hz, J_{XB} = 12.3 Hz), 6.92 (d, 2H, Ar–H, J = 8.4 Hz), 7.12 (d, 2H, Ar–H, J = 8.3 Hz), 7.31 (m, 2H, C5–H chromene and C6–H chromene), 7.52 (t, 1H, C7–H chromene, J = 7.2 Hz), 7.83 (d, 1H, C8–H chromene, J = 8.1 Hz), 8.52 (s, 1H, C4–H chromene). Anal. calculated for $C_{21}H_{14}FN_3O_3S$ (407.42): C, 61.91; H, 3.46; N, 10.31. Found: C, 61.97; H, 3.57; N, 10.41.

4.1.5. General procedure for the synthesis of 3-(1-(4-(4-Bromophenyl)thiazol-2-yl)-5-(4-(un)substituted phenyl)-4,5-dihydro-1*H*-pyrazol-3-yl)-2*H*-chromene-2-one (5a–c). 2-Bromo-1-(4-bromophenyl)ethanone (1.72 g, 10 mmol) was added to a solution of the appropriate thiocarbomoyl-pyrazoline derivative **3a,b,f** (10 mmol) in absolute ethanol (30 mL) in the presence of hydrochloric acid (2 mL) and refluxed for 12 h (TLC). The solid product was filtered, dried and crystallized from DMF/ethanol.

*4.1.5.1 3-(1-(4-(4-Bromophenyl)thiazol-2-yl)-5-phenyl-4,5-dihydro-1H-pyrazol-3-yl)-2H-chromene-2-one (**5a**):.* Yield %: 76, m.p. 276–179 °C. IR ν_{max} cm^{-1}: 2933 (CH aliphatic), 3051 (CH aromatic), 1726 (C═O chromene), 1602, 1495 (C═C, C═N).^{1}H-NMR ($CDCl_3$ 400 MHz), δ ppm: 3.72 (dd, 1H, C4–H_A pyrazoline, J_{AX} = 5.2 Hz, J_{AB} = 18.2Hz), 4.15 (dd, 1H, C4–H_B pyrazoline, J_{BX} = 11.3 Hz, J_{BA} = 18.2 Hz), 5.78 (dd, 1H, C5–H_X pyrazoline, J_{XA} = 5.2 Hz, J_{XB} = 11.3 Hz), 6.88 (CH thiazole), 6.92 (d, 2H, Ar–H, J = 8.4 Hz), 7.38 (m, 4H, Ar–H, C5–H and C6–H chromene), 7.52 (d, 2H, Ar–H, J = 8.4 Hz), 7.64 (m, 4H, Ar–H and C7–H chromene), 7.77 (d, 1H, C8–H chromene, J = 7.6 Hz), 8.61 (s, 1H, C4–H chromene). Anal. calculated for $C_{27}H_{18}BrN_3O_2S$ (528.42): C, 61.37; H, 3.43; N, 7.95. Found: C, 61.45; H, 3.56; N, 8.01.

*4.1.5.2 3-(1-(4-(4-Bromophenyl)thiazol-2-yl)-5-(4-methoxyphenyl)-4,5-dihydro-1H-pyrazol-3-yl)-2H-chromene-2-one (**5b**).* Yield %: 76, m.p. 286–188 °C. IR ν_{max} cm^{-1}: 2933 (CH aliphatic), 1726 (C═O chromene), 1602, 1495 (C═C, C═N). ^{1}H-NMR ($CDCl_3$ 400 MHz), δ ppm: 3.61 (dd, 1H, C4–H_A pyrazoline, J_{AX} = 6.7 Hz, J_{AB} = 18.8 Hz), 3.81 (s, 3H, OCH_3), 4.15 (dd, 1H, C4–H_B pyrazoline, J_{BX} = 12.2 Hz, J_{BA} = 18.8 Hz), 5.69 (dd, 1H, C5–H_X pyrazoline, J_{XB} = 12.2 Hz, J_{XA} = 6.7 Hz), 6.84 (CH thiazole), 6.90 (d, 2H, Ar–H, J = 8.7 Hz), 7.35–7.38 (m, 4H, Ar–H, C5–H and C6–H chromene), 7.47 (d, 2H, Ar–H, J = 8.6 Hz), 7.57–7.60 (m, 3H, Ar–H and C7–H chromene), 7.64 (d, 1H, C8–H chromene, J = 7.7 Hz), 8.50 (s, 1H, C4–H chromene). ^{13}C-NMR (DMSO 100.63 MHZ): 45.25 (C-4 pyrazoline), 55.27 (OCH_3), 64.87 (C-5 pyrazoline), 104.02 (CH thiazole), 112.82, 114.06, 116.02, 117.79, 119.07, 119.59, 121.58, 123.70, 124.86, 127.56, 128.45, 128.73, 132.50, 133.11, 135.51, 140.19, 153.98, 159.25, 159.35 (aromatic C), 164.48 (carbonyl). Anal. calculated for $C_{28}H_{20}BrIN_3O_3S$ (685.35): C, 60.22; H, 3.61, 14.31; N, 7.52. Found: C, 60.31; H, 3.69; N, 7.58.

*4.1.5.3 3-(1-(4-(4-Bromophenyl)thiazol-2-yl)-5-(4-fluorophenyl)-4,5-dihydro-1H-pyrazol-3-yl)-2H-chromene-2-one (**5c**):.* Yield %: 81, m.p. 282–285 °C. IR ν_{max} cm^{-1}: 2933 (CH aliphatic), 1726 (C═O chromene), 1602, 1515 (C═C, C═N). ^{1}H-NMR ($CDCl_3$ 400 MHz), δ ppm: 3.64 (dd, 1H, C4–H_A pyrazoline, J_{AX} = 6.3 Hz, J_{AB} = 19.0 Hz), 4.19 (dd, 1H, C4–H_B pyrazoline, J_{BX} = 11.9 Hz, J_{BA} = 18.9 Hz), 5.95 (dd, 1H, C5–H_X pyrazoline, J_{XA} = 6.2 Hz, J_{XB} = 11.3 Hz), 6.85 (CH thiazole), 6.92 (t, 2H, Ar–H, J = 8.6 Hz), 7.36–7.50 (m, 4H, 4Ar–H, C5–H and C6–H chromene), 7.56–7.68 (m, 4H, 2Ar–H, C7–H chromene and C8–H chromene), 8.55 (s, 1H, C4–H chromene). Anal. Calculated for $C_{27}H_{17}BrFN_3O_2S$ (546.41): C, 59.35; H, 14.62; N, 7.69. Found: C, 59.39; H, 14.67; N, 7.73.

4.2. Anticancer activity study

4.2.1. MTT assay for *in vitro* cytotoxicity. Antiproliferative activity of the target compounds was determined in cells treated with different concentrations of the tested compounds in comparison with an untreated control using MTT assay as follows:

Cells were grown as monolayers in media supplemented with 10% inactivated fetal bovine serum. The monolayers of 10 000 cells were plated (10^4 cells per well) in a 96-well tissue culture plate and incubated for 24 h at 37 °C in a humidified incubator with 5% CO_2 before treatment with the compounds to allow attachment of cells to the plate except blank wells without cells. Different concentrations of 100, 10, 1.0, 0.1 and 0.01 μM of each compound were tested for cytotoxicity. Tetraplicate wells were prepared for each concentration in addition to cell controls (cells only without compounds). Cells were incubated with the tested compounds for 48 h in a CO_2 incubator at 37 °C and 5% CO_2. Culture media containing different concentrations of the tested compounds and dead cells were decanted leaving only viable attached cells in the tissue culture plate. The plate was washed twice with pre-warmed PBS. MTT reagent (40 μl) was added to each well including blank and negative control wells. After the addition of MTT reagent the plates were incubated in the dark for 4 h for the reduction of MTT into formazan (purple color) by dehydrogenase activity in the mitochondria of viable cells.

DMSO (150 μL) was added to each well to solubilize the purple crystals of formazan. Absorbance was measured at 570 nm using a microplate reader (ROBONIK TM P2000 Eliza plate reader). The percentage of cell survival was calculated as [(Absorbance of Sample − Absorbance of Blank)/(Absorbance of Control − Absorbance of Blank)] ×100. The inhibitory concentration 50 (IC_{50}) was calculated by plotting log molar concentration of the tested compounds against survival rate percent.

4.2.2. *In vitro* EGFR inhibition assay in MCF-7 cell line. The cells in culture medium were treated with 20 μL of IC_{50} values of the tested compounds or the standard drug doxorubicin dissolved in DMSO, then incubated for 24 h at 37 °C in a humidified 5% CO_2 atmosphere. The cells were harvested, and homogenates were prepared in saline using a tight pestle homogenizer until complete cell disruption. The kit uses a double antibody sandwich enzyme-linked immunosorbent assay (ELISA) to assay the level of human EGFR in the samples. A monoclonal antibody for EGFR has been precoated onto 96-well plates. Standard and test samples are added to the wells, biotinylated detection polyclonal antibodies from goat specific for EGFR are added subsequently and followed by washing with PBS buffer. The avidin–biotin–peroxidase complex was added, and unbound conjugates were washed away with PBS buffer. HRP substrate TMB was used to visualize HRP enzymatic reaction. TMP was catalyzed by HRP to produce a blue color product that changed into yellow after adding acidic stop solution. The density of yellow is proportional to the human EGFR amount of sample captured in the plate. The chroma of color and the concentration of human EGFR of samples were positively correlated and the optical density was determined at 451 nm. The level of human EGFR was calculated (pg. mL^{-1}) as duplicate determinations from the standard curve.

4.2.3. Cell cycle analysis. The breast cancer cells (MCF-7) were exposed to the IC_{50} dose of **3d** (0.005 μM) and **5a** (0.020 μM) or to DMSO (0.002%) as a control for 24 h. Treated cells then were suspended in 0.5 mL of PBS, centrifuged, collected and fixed in ice/cold ethanol (70% v/v) for 2 h at 4 °C then, they were washed with PBS, suspended using 0.1 mg mL^{-1} RNase and stained with 40 $mgmL^{-1}$ PI. Flow cytometry analysis was performed using the FACScalibur (Becton Dickinson) and Phoenix Flow Systems and Verity Software House was used for the cell cycle distribution calculations.[33]

4.2.4. Annexin V–FITC apoptosis assay. The breast cancer cells (MCF-7) were exposed to the IC_{50} dose of **3d** (0.005 μM) and **5a** (0.020 μM) or to DMSO (0.002%) as a control for 24 h. Treated cells then were suspended in 0.5 mL of PBS, centrifuged, collected and fixed in ice/cold ethanol (70% v/v) for 2 h at 4 °C. Subsequently, the cells were washed with PBS and centrifuged. The cells were stained using a mixture of fluorescein isothiocyanate (FITC), annexin V (component no. 51-65875X) and propidium iodide (PI) and suspended in the dark at 37 °C for 30 min. Flow cytometry analysis was performed using the FACScalibur (Becton Dickinson) and Phoenix Flow Systems and Verity Software House was used for the cell cycle distribution calculations.[34]

4.2.5. Molecular docking. Docking was performed *via* Autodock Vina.[35] The crystal structure of the target tyrosine kinase in complex with erlotinib, PDB ID: 1M17, was prepared using UCSF Chimera.[36] Gasteiger charges were used for the protein and all the ligands. The ligands were first docked while fixing the coordinates of the side chains of the ATP, or erlotinib, binding site and then repeated with flexible side chains. All amino acids within 5 Å of erlotinib were considered flexible in the flexible protocol. Docking was performed on a dry active site; that is, all the water was removed. The results were visualized using UCSF Chimera and ligplot+.[37]

4.2.6. Molecular dynamics. Topology and coordinate files were prepared *via* Amber tools 14.[38] Three dynamics trajectories were run for the protein in complex with erlotinib, **3d** and **5a**. The erlotonib run serves as a control reference. In all cases, the chain that joins tyrosine kinase to the transmembranal domain was excised. The crystal structure for erlotinib was used and prepared using the pdb4amber and reduce programs.[39] For **3d** and **5a**, the best docked-poses were used and the protein was similarly processed for use in Amber. The all-atom forcefield AMBER ff12SB[40,41] was universally used. As the forcefield does not contain parameters for the ligand, all ligands were parameterized using ANTECHAMBER[42] to generate parameters that are consistent with the General Amber Force Field (GAFF).[43] The AM1-BCC method was used to assign charges. Crystallographic waters were retained and each protein was solvated with approximately 24480 TIP3P water molecules in a 100x100x88 A3 box. Three Cl-ions were added to neutralize the positively-charged protein and 68 additional NaCl ions were added to reach a salt concentration of 0.15 mM.

MD simulations were carried out using the AMBER Molecular Dynamics package[38] following a standard protocol adopted of minimization, heating, density equilibration and production. The AMBER input files are similar to those in the ESI of the previous work of Salem and Brown[44] with only changing the relevant number of residues whenever restraints are applied. The trajectory lengths for heating, density equilibration and production were 20 ps, 50 ps and 10 ns, respectively. As can be inferred from the input files, Langevin dynamics were generally employed. The trajectories were analyzed using CPPTraj,[45] XMgrace[46] and VMD.[47] The RMSD plot was calculated for residues ARG681 to VAL956, as the other residues belong to highly flexible loops that are far from the binding site and add significant noise to the plots.

Conflicts of interest

The authors declare that they have no conflict of interest.

Acknowledgements

This research was enabled in part by support provided by Westgrid (www.westgrid.ca) and Compute/Calcul Canada (www.computecanada.ca). Access to westgrid was provided through collaboration with Professor Alex Brown, University of Alberta.

References

1 K. N. Venugopala, V. Rashmi and B. Odhav, Review on natural coumarin lead compounds for their pharmacological activity, *BioMed Res. Int.*, 2013, **2013**, 963248.

2 X. Wang, K. F. Bastow, C. M. Sun, Y. L. Lin, H. J. Yu, M. J. Don, T. S. Wu, S. Nakamura and K. H. Lee, Antitumor Agents. 239. Isolation, Structure Elucidation, Total Synthesis, and Anti-Breast Cancer Activity of Neo-tanshinlactone from Salvia miltiorrhiza, *J. Med. Chem.*, 2004, **47**(23), 5816–5819.

3 K. V. Sashidhara, J. N. Rosaiah, M. Kumar, R. K. Gara, L. V. Nayak, K. Srivastava, H. K. Bid and R. Konwar, Neotanshinlactone inspired synthesis, in vitro evaluation of novel substituted benzocoumarin derivatives as potent anti-breast cancer agents, *Bioorg. Med. Chem. Lett.*, 2010, **20**(23), 7127–7131.

4 H. Brady, S. Desai, L. M. Gayo-Fung, S. Khammungkhune, J. A. McKie, E. O'Leary, L. Pascasio, M. K. Sutherland, D. W. Anderson, S. S. Bhagwat and B. Stein, Effects of SP500263, a novel, potent antiestrogen, on breast cancer cells and in xenograft models, *Cancer Res.*, 2002, **62**(5), 1439–1442.

5 F. Leonetti, A. Favia, A. Rao, R. Aliano, A. Paluszcak, R. W. Hartmann and A. Carotti, Design, Synthesis, and 3D QSAR of Novel Potent and Selective Aromatase Inhibitors, *J. Med. Chem.*, 2004, **47**(27), 6792–6803.

6 S. J. Stanway, A. Purohit, L. L. Woo, S. Sufi, D. Vigushin, R. Ward, R. H. Wilson, F. Z. Stanczyk, N. Dobbs, E. Kulinskaya, M. Elliott and I. Phase, Study of STX 64 (667 Coumate) in Breast Cancer Patients: The First Study of a Steroid Sulfatase Inhibitor, *Clin. Cancer Res.*, 2006, **12**(5), 1585–1592.

7 M. A. Musa, J. S. Cooperwood and M. O. F. Khan, A review of coumarin derivatives in pharmacotherapy of breast cancer, *Curr. Med. Chem.*, 2008, **15**(26), 2664–2679.

8 M. P. Thomas and B. V. L. Potter, Discovery and Development of the Aryl O-Sulfamate Pharmacophore for Oncology and Women's Health, *J. Med. Chem.*, 2015, **58**(19), 7634–7658.

9 C. Palmieri, R. C. Stein and X. Liu, *et al.*, IRIS study: a phase II study of the steroid sulfatase inhibitor Irosustat when added to an aromatase inhibitor in ER-positive breast cancer patients, *Breast Cancer Res. Treat.*, 2017, **165**(2), 343–353.

10 C. Palmieri, R. Stein, X. Liu, E. Hudson and S. Reed, A Phase II study to assess the safety and efficacy of the steroid sulfatase inhibitor Irosustat when added to an aromatase inhibitor in ER positive locally advanced or metastatic breast cancer patients (IRIS) – Trial Results, *J. Clin. Oncol.*, 2016, **34**, 549.

11 A. Stefanachi, A. D. Favia, O. Nicolotti, F. Leonetti, L. Pisani, M. Catto, C. Zimmer, R. W. Hartmann and A. Carotti, Design, Synthesis, and Biological Evaluation of Imidazolyl Derivatives of 4,7-Disubstituted Coumarins as Aromatase Inhibitors Selective over 17-α-Hydroxylase/C17–20 Lyase, *J. Med. Chem.*, 2011, **54**(6), 1613–1625.

12 N. S. Reddy, K. Gumireddy, M. R. Mallireddigari, S. C. Cosenza, P. Venkatapuram, S. C. Bell, E. P. Reddy and M. R. Reddy, Novel coumarin-3-(N-aryl)carboxamides arrest breast cancer cell growth by inhibiting ErbB-2 and ERK1, *Bioorg. Med. Chem.*, 2005, **13**(9), 3141–3147.

13 N. Normanno, A. De Luca, C. Bianco, L. Strizzi, M. Mancino, M. R. Maiello, A. Carotenuto, G. De Feo, F. Caponigro and D. S. Salmon, Epidermal growth factor receptor (EGFR) signaling in cancer, *Gene*, 2006, **366**(1), 2–16.

14 B. P. Bandgar, J. V. Totre, S. S. Gawande, C. N. Khobragade, S. C. Warangkar and P. D. Kadam, Synthesis of novel 3,5-diaryl pyrazole derivatives using combinatorial chemistry as inhibitors of tyrosinase as well as potent anticancer, anti-inflammatory agents, *Bioorg. Med. Chem.*, 2010, **18**(16), 6149–6155.

15 X. H. Liu, B. F. Ruan, J. X. Liu, B. A. Song, L. H. Jing, J. Li, Y. Yang, H. L. Zhu and X. B. Qi, Design and synthesis of N-phenylacetyl (sulfonyl) 4,5-dihydropyrazole derivatives as potential antitumor agents, *Bioorg. Med. Chem. Lett.*, 2011, **21**(10), 2916–2920.

16 C. Blackburn, M. O. Duffey, A. E. Gould, B. Kulkarni, J. X. Liu, S. Menon, M. Nagayoshi, T. J. Vos and J. Williams, Discovery and optimization of N-acyl and N-aroylpyrazolines as B-Raf kinase inhibitors, *Bioorg. Med. Chem. Lett.*, 2010, **20**(16), 4795–4799.

17 Y. Garazd, M. Garazd and R. Lesyk, Synthesis and evaluation of anticancer activity of 6-pyrazolinylcoumarin derivatives, *Saudi Pharm. J.*, 2017, **25**(2), 214–223.

18 S. L. BullPhelps, J. O. Schorge, M. J. Peyton, H. Shigematsu, L. Xiang, D. S. Miller and J. S. Lea, Implications of EGFR inhibition in ovarian cancer cell proliferation, *Gynecol. Oncol.*, 2008, **109**(3), 411–417.

19 T. Fozing, C. Scheuer and S. Samnick, Synthesis and initial tumor affinity testing of iodine-123 labelled EGFR-affine agents as potential imaging probes for hormone-refractory prostate cancer, *Eur. J. Med. Chem.*, 2010, **45**(9), 3780–3786.

20 W. Yang, Y. Hu, Y. Yang, F. Zhang, Y. Zhang, X. Wang, J. Tang, W. Zhong and H. Zhu, Design, modification and 3D QSAR studies of novel naphthalin-containing pyrazoline derivatives with/without thiourea skeleton as anticancer agents, *Bioorg. Med. Chem.*, 2013, **21**(5), 1050–1063.

21 P. C. Lv, D. D. Li, Q. S. Li, X. Lu, Z. P. Xiao and H. L. Zhu, Synthesis and biological evaluation of pyrazole derivatives containing thiourea skeleton as anticancer agents, *Bioorg. Med. Chem.*, 2010, **18**(13), 4606–4614.

22 P.-C. Lv, D. D. Li, Q. S. Li, X. Lu, Z. P. Xiao and H. L. Zhu, Synthesis, molecular docking and evaluation of thiazolylpyrazoline derivatives as EGFR TK inhibitors and potential anticancer agents, *Bioorg. Med. Chem. Lett.*, 2011, **21**(18), 5374–5377.

23 D. Havrylyuk, B. Zimenkovsky, O. Vasylenko, L. Zaprutko, A. Gzella and R. Lesyk, Synthesis of novel thiazolone-based compounds containing pyrazoline moiety and evaluation of their anticancer activity, *Eur. J. Med. Chem.*, 2009, **44**(4), 1396–1404.

24 F. A. Ragab, A. A. M. Eissa, S. H. Fahim, M. A. Salem, M. A. Gamal and Y. M. Nissan, Synthesis and biological evaluation of new coumarin derivatives as cytotoxic agents, *Arch. Pharm.*, 2021, e2100029.
25 N. Kumar, Synthesis of 3-substituted phenyl-1-(3-coumarinyl)-propan-1-one derivative using secondary amine catalysts, *World Res. J. Biochem.*, 2012, **1**(1), 20–26Available.
26 E. Bombardelli and P. Valenti, *US Pat.*, 6767916, 2004.
27 K. V. Sashidhara, A. Kumar, M. Kumar, J. Sarkar and S. K. Sinha, *US Pat.*, 8815940, 2014.
28 M. V. Berridge, P. M. Herst and A. S. Tan, Tetrazolium dyes as tools in cell biology: New insights into their cellular reduction, *Biotechnol. Annu. Rev.*, 2005, **11**, 127–152.
29 M. T. T. Cell Proliferation Assay available online at www.atcc.org.
30 Enzyme-linked Immunosorbent Assay Kit available online at www.arp1.com.
31 A. Wissner, D. M. Berger, D. H. Boschelli, M. B. Floyd, L. M. Greenberger, B. C. Gruber, B. D. Johnson, N. Mamuya, R. Nilakantan, M. F. Reich, R. Shen, H. Tsou, E. Upeslacis, Y. F. Wang, BYe Fei Wu and N. Zhang, 4-Anilino-6,7-dialkoxyquinoline-3-carbonitrile Inhibitors of Epidermal Growth Factor Receptor Kinase and Their Bioisosteric Relationship to the 4-Anilino-6,7-dialkoxyquinazoline Inhibitors, *J. Med. Chem.*, 2000, **43**(17), 3244–3256.
32 J. Stamos, M. X. Sliwkowski and C. Eigenbrot, Structure of the epidermal growth factor receptor kinase domain alone and in complex with a 4-anilinoquinazoline inhibitor, *J. Biol. Chem.*, 2002, **277**(48), 46265–46272.
33 I. Nicoletti, G. Migliorati, M. C. Pagliacci, F. Grignani and C. Riccardi, A rapid and simple method for measuring thymocyte apoptosis by propidium iodide staining and flow cytometry, *J. Immunol. Methods*, 1991, **139**, 271–279.
34 I. Vermes, C. Haanen, H. Steffens-Nakken and C. Reutelingsperger, A novel assay for apoptosis. Flow cytometric detection of phosphatidylserine expression on early apoptotic cells using fluorescein labelled Annexin V, *J. Immunol. Methods*, 1995, **184**, 39–51.
35 O. Trott and A. J. Olson, AutoDock Vina: improving the speed and accuracy of docking with a new scoring function, efficient optimization, and multithreading, *J. Comput. Chem.*, 2010, **31**(2), 455–461.
36 E. F. Pettersen, T. D. Goddard, C. C. Huang, G. S. Couch, D. M. Greenblatt, E. C. Meng and T. E. Ferrin, UCSF Chimera–a visualization system for exploratory research and analysis, *J. Comput. Chem.*, 2004, **25**(13), 1605–1612.
37 R. A. Laskowski and M. B. Swindells, LigPlot +: multiple ligand-protein interaction diagrams for drug discovery, *J. Chem. Inf. Model.*, 2011, **51**(10), 2778–2786.
38 D. A. Case, T. Darden, T. Cheatham III, C. Simmerling, J. Wang, R. Duke, R. Luo, R. Walker, W. Zhang, K. Merz, B. Roberts, S. Hayik, A. Roitberg, G. Seabra, J. Swails, A. Goetz, I. Kolossvary, K. Wong, F. Paesani, J. Vanicek, R. Wolf, J. Liu, X. Wu, S. Brozell, T. Steinbrecher, H. Gohlke, Q. Cai, X. Ye, J. Wang, M. Hsieh, G. Cui, D. Roe, D. Mathews, M. Seetin, R. Salomon-Ferrer, C. Sagui, V. Babin, T. Luchko, S. Gusarov, A. Kovalenko and P. Kollman. *AMBER 12*, University of California, San Francisco, 2012.
39 J. M. Word, S. C. Lovell, J. S. Richardson and D. C. Richardson, Asparagine and glutamine: using hydrogen atom contacts in the choice of side-chain amide orientation, *J. Mol. Biol.*, 1999, **285**(4), 1735–1747.
40 W. D. Cornell, P. Cieplak, C. I. Bayly, I. R. Gould, K. M. Merz, D. M. Ferguson, D. C. Spellmeyer, T. Fox, J. W. Caldwell and P. A. Kollman, A Second Generation Force Field for the Simulation of Proteins, Nucleic Acids, and Organic Molecules, *J. Am. Chem. Soc.*, 1995, **117**(19), 5179–5197.
41 V. Hornak, R. Abel, A. Okur, B. Strockbine, A. Roitberg and C. Simmerling, Comparison of multiple Amber force fields and development of improved protein backbone parameters, *Proteins: Struct., Funct., Bioinf.*, 2006, **65**(3), 712–725.
42 J. Wang, W. Wang, P. A. Kollman and D. A. Case, Automatic atom type and bond type perception in molecular mechanical calculations, *J. Mol. Graphics Modell.*, 2006, **25**(2), 247–260.
43 J. Wang, R. M. Wolf, J. W. Caldwell, P. A. Kollman and D. A. Case, Development and testing of a general amber force field, *J. Comput. Chem.*, 2004, **25**(9), 1157–1174.
44 M. A. Salem and A. Brown, Two-photon absorption of fluorescent protein chromophores incorporating non-canonical amino acids: TD-DFT screening and classical dynamics, *Phys. Chem. Chem. Phys.*, 2015, **17**(38), 25563–25571.
45 D. R. Roe and T. E. Cheatham, PTRAJ and CPPTRAJ: Software for Processing and Analysis of Molecular Dynamics Trajectory Data, *J. Chem. Theory Comput.*, 2013, **9**(7), 3084–3095.
46 P. J. Turner, *XMGRACE, Version 5.1.19.*, Center for Coastal and Land-Margin Research, Oregon Graduate Institute of Science and Technology, Beaverton, Oregon.
47 W. Humphrey, A. Dalke and K. Schulten, VMD: visual molecular dynamics, *J. Mol. Graphics Modell.*, 1996, **14**(1), 27–2833–8.